Effects of density on the mechanical properties of spark plasma sintered β-SiC

Florimond Delobel, Sébastien Lemonnier, Julien Cambedouzou

Version of Record: https://www.sciencedirect.com/science/article/pii/S0272884220304235
Manuscript_43f28e346e3a178adcae235e8673fc18

Effects of density on the mechanical properties of spark plasma sintered β-SiC

Florimond Delobel [a, b, *], Sébastien Lemonnier [a, *], Julien Cambedouzou [b, c]

[a] French-German research Institute of Saint-Louis, Saint-Louis, France
[b] ICSM, CEA, CNRS, ENSCM, Univ Montpellier, Marcoule, France
[c] IEM, CNRS, ENSCM, Univ Montpellier, Montpellier, France
* Corresponding authors: f.delobel@bcrc.be, sebastien.lemonnier@isl.eu

Abstract

The influence of density on the hardness value of β-SiC samples was studied based on Knoop and Vickers indentation tests. Hardness measurements were performed on additive-free spark plasma sintered SiC samples in the [80%-95%] density range and on highly dense samples (>99%) sintered with very low content of sintering aids. Results revealed that the density has a strong influence on the hardness value, which increases of about 7GPa between samples presenting densities of 80% and 95% and even reaches 21GPa under 2kg with Knoop indenter for the densest samples sintered with very low content of sintering aids. These results allowed us to give a comprehensive model-supported analysis of the mechanical properties of spark plasma sintered β-SiC with controlled porosity that currently does not exist in the literature. The calculation of Young modulus and toughness further resulted in encouraging properties for our samples with regards to mechanical and ballistic performances.

Keywords: Silicon Carbide, Mechanical testing, Hardness, Toughness, Young modulus

1 Introduction

Silicon carbide (SiC) attracts considerable attention in the field of materials research due to its exceptional mechanical, thermal and electronic properties [1]. Thanks to its high hardness and low density, this ceramic material presents a great interest for ballistic protection, especially in dual hardness armour [2]. Indeed, these properties allow it to be as competitive as other

carbides against small-calibre projectiles or Armor-Piercing Fin Stabilized Discarding sabot while presenting much lower cost [2]. Moreover, Chen et al. demonstrated an amorphization phenomenon for boron carbide against heavy core projectile, as tungsten carbide, which does not appear in SiC pellets, making it more efficient against this kind of threat [3].

The cubic form of SiC is particularly appreciated to confer isotropic properties and better hardness than the hexagonal structure [4]. The isotropic properties of cubic SiC also make this material really interesting for other applications in high power electronics and extreme specific stiffness materials. Nevertheless, in the literature, SiC developed for ballistic applications are never composed of β-SiC due to densification limitations, which are critical for performances. Indeed, the covalent character of its chemical bonds makes its sintering very difficult [1] and full density was only reported at very high temperature and/or with sintering aids [5]–[7]. The sintering of SiC at very high temperature (>1900°C) could induce a phase transition into hexagonal polytype. Furthermore, the use of sintering aids leads to the presence of secondary phases, which could be detrimental for mechanical properties due to their lower hardness than pristine SiC. Thanks to its isotropic properties and high hardness, it appears particularly interesting to maintain the cubic phase of SiC for ballistic applications and a solution based on several studies reported in the literature should be the use of nanometric SiC powders since they were found to exhibit high sintering reactivity limiting, even avoiding the need for sintering additive during the fabrication of highly dense samples [8]–[11].

Baumann was the first author who reported the cubic into hexagonal transition at the temperature of 2100°C, which is typical temperature for SiC sintering [5]–[7], [12]. Nevertheless, other works generally reported the temperature of 1900°C for this transition, especially in the case where the presence of defects (stacking faults) was verified in the crystalline structure of SiC [13], [14]. On the other hand, thermodynamical studies of Sugiyama and Togaya evidenced the impact of gas pressure on the 3C-6H SiC transition [15]. These works showed that applying high pressure can stabilize the β-SiC polytype and delay the transition at higher temperature. In addition, we have recently demonstrated the role of sintering pressure on the cubic into hexagonal transition [16]. Indeed, we showed the possibility to stabilize the cubic form of SiC at higher temperature by applying high sintering pressure while increasing the density of SiC pellets up to 95% of theoretical density (T.D.).

In addition to the effect of porosity, the grain size also influences the value of the hardness of ceramic materials, as generally reported in the literature, and particularly by the empirical Hall-Petch law [17]. Indeed, the decrease of grain size increases the number of grain boundaries, which create structural obstructions to cracks propagation and improves the elasticity limit of the material, and thus its hardness. Moreover, a decrease of grain size also allows reducing

the density of local dislocations and thus improves the elasticity limit and hardness of the material. This demonstrates that the hardness of a polycrystalline ceramic is improved by the refinement of its microstructure [10]. The use of nanometric powder is thus desirable in order to conserve fine microstructure and improve mechanical properties of SiC compacts.

The goal of this work is to investigate the relationships between cubic SiC sample hardness and density. The obtained trends will therefore be discussed based on different empirical models reported in the literature. Hardness measurements and derived SiC mechanical properties (Young modulus and toughness) will then be compared with the ones referenced in the literature in order to assess the ballistic performance of our samples. Finally, experimentations on highly dense samples obtained by spark plasma sintering (SPS) with very low content of sintering aids will be displayed.

2 Experimental

2.1 Materials

The starting materials used in this study are a high purity (>98%) commercial β-SiC powder produced by laser pyrolysis, with an average grain size of 35 nm, which was purchased from Nanomakers (France), a high purity α-Al_2O_3 powder (99.9%), with an average grain size lower than 1µm, purchased from Alfa Aesar, a high purity Y_2O_3 powder (99.995%), with an average grain size of 60nm, purchased from Alfa Aesar and a high purity AlN powder (> 99%), with an average grain size lower than 100nm, purchased from Sigma Aldrich company.

Undoped sintered samples are studied in section 3.1., while section 3.2. is dedicated to different “SiC powder + sintering aid” mixtures performed after blending in a three-dimensional blender during 1 hour at 49 rpm. The used powder masses and the denomination of the mixtures are reported in Table 1. The mixtures with Al_2O_3/Y_2O_3 and Al_2O_3/AlN components respectively involve mass ratios of 63wt%/37wt% and 50wt%/50wt%.

Table 1 – Table of SiC shades doped with three sintering aids denomination and weight contents.

Added sintering aid	Name of the mixture	Aid content (wt%)	Powder mass (g)	
			SiC	Sintering aid
Al_2O_3	NMK-A50	0.5	9.95	0.05
Al_2O_3/Y_2O_3	NMK-AY50	0.5	9.95	0.05
Al_2O_3/AlN	NMK-NA50	0.5	9.95	0.05

2.2 Sintering parameters

SPS was performed to consolidate both powders using a SPS HP D125 apparatus from FCT Systeme GmbH. The SiC powders were introduced in a graphite die with an inner diameter of 30 mm. Three layers of graphite felt with a thickness of 6 mm were wrapped around the graphite die and two other layers were put over and under it to limit thermal losses during sintering. A cold pre-compaction at 100 kg/cm² was applied to keep the system in. Then, the latter was heated using DC pulse current. An optical pyrometer was used to control temperature at a distance of 3 mm from the sample through a hole in the upper puncher, this configuration ensuring a reliable measurement of sample temperature.

Samples were sintered with a temperature ranging from 1850°C to 2200°C using a heating rate of 10°C/min under vacuum atmosphere. Various sintering pressures from 17 to 127MPa were applied and a dwell of 10 minutes at maximum temperature was set. Please note that an intermediary pressure of 50MPa was applied at the beginning of the sintering test, excepted for experiments under 17MPa where the pressure stayed constant during the entire test. The maximal sintering pressure was then applied in four minutes between 1160°C and 1200°C, just before the beginning of the sintering of the powder. The pressure was released at the end of the dwell time and the cooling step was not controlled.

2.3 Physical, chemical and mechanical characterizations

A D8 Advance Bruker AXS device (Cu Kα radiation, λ = 0.154 nm) was used for X-ray diffraction analyses. SEM observations were performed using a Nova Nanosem 450 FEI apparatus with CBS detector. The densities of sintered samples were measured by the Archimede's method.

Hardness tests (Knoop and Vickers indenters) were performed by a Buehler micro-durometer with OmniMet HMS software. Each hardness value presented in the following corresponds to the average of ten indentations, each one being measured twice with two different focuses in

order to limit the dependence of the measurement regarding the operator. Young modulus and toughness of all samples were respectively calculated using Knoop and Vickers hardness measurements. Two models were used to calculate Young modulus: the Marshall's relation [18], which shows that there is a relation linking the Young modulus E and the small/great print diagonal ratio, and the Pabst's relation [19], which takes into account the porosity as main factor affecting the Young modulus. Toughness was determined after measurement of print diagonals and cracks that appear all around it thanks to the works of Niihara et al., Anstis et al., and Evans and Charles [20]–[23]. More details about the calculation of these two properties are given in the following of this paper.

3 Results and discussion

3.1 Additive-free sintered samples

3.1.1 Hardness measurements

In order to characterize hardness properties of samples sintered from commercial SiC powder (called NMKSiC), four pristine cubic pellets were studied. These samples, respectively presenting densities of 80%, 85%, 90% and 95% of T.D. and called NMK80, NMK85, NMK90 and NMK95, allow evaluating the influence of microstructure and porosity on the hardness values. The SEM micrographs of these four samples are presented in Figure 1. The obtained microstructures, only composed by equiaxed grains, combined with the experimental XRD patterns (Figure 3), testify to the presence of a pristine cubic crystalline structure for these sintered samples.

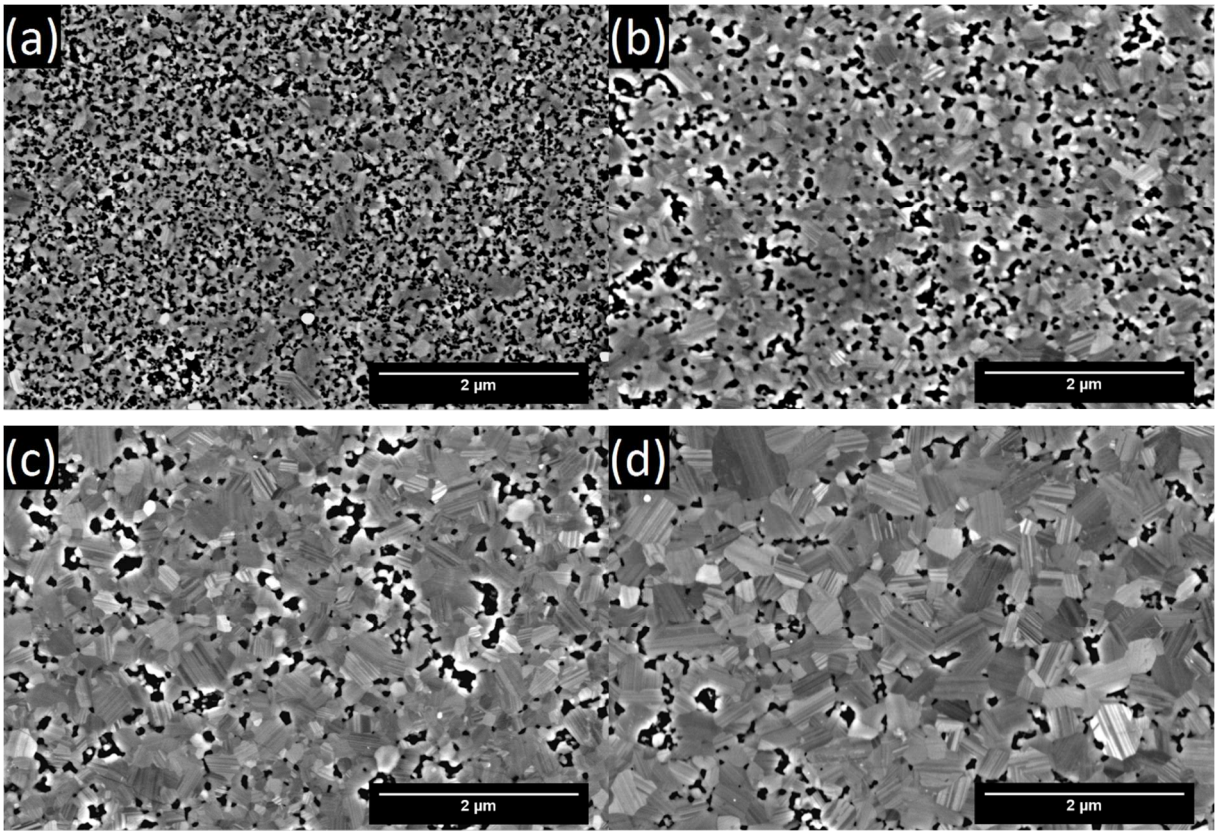

Figure 1 – SEM micrographs of the pristine cubic samples denoted (a) NMK-80, (b) NMK-85, (c) NMK-90 and (d) NMK-95

In addition of the equiaxed grain shape, the SEM micrographs of the four pristine cubic samples (Figure 1) show an increase of the grain size according to the increase of the density. This grain growth can be attributed to the sintering conditions adaptation since the bulk density gains were achieved by means of sintering temperature increase and/or longer dwell time. Figure 2 shows the evolution of grain size of the four characteristic pristine cubic samples according to their density. It is possible to observe that the average grains size increases from 160nm to 320nm according to an exponential law respectively for samples presenting densities of 80% and 95% of T.D.. Nevertheless, the microstructures of these four samples remain highly fine compared to the ones reported in the literature [24], [25] and suggest promising mechanical properties.

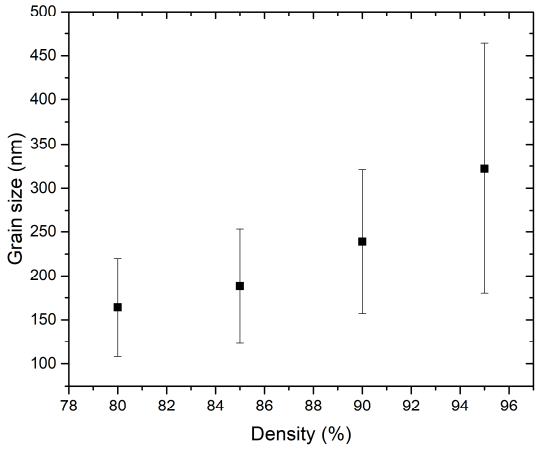

Figure 2 - Evolution of grain size of the four pristine cubic sintered sample according to their density

Figure 1 finally shows the presence of twins, especially for samples NMK-90 and NMK-95. These twins represent structural defects in the material The presence of structural defects is also noticed by the peak of stacking faults in the experimental XRD patterns (Figure 3). These twins are originating from the presence of stacking faults in the raw powder but also from the application of pressure during sintering that increases the density of defects in the samples. Indeed, Figure 3 only shows a shouldering for the indication of stacking faults in the raw powder, while the four samples present a well-defined peak at a scattering angle of $2\theta = 33.6°$ that could testify to an increase of their density.

Figure 3 also shows wider peaks for the raw powder compared to the ones of the sintered samples NMK-80, NMK-85, NMK-90 and NMK-95. This indicates an increase in terms of crystallite size during sintering between the raw powder and the sintered samples.

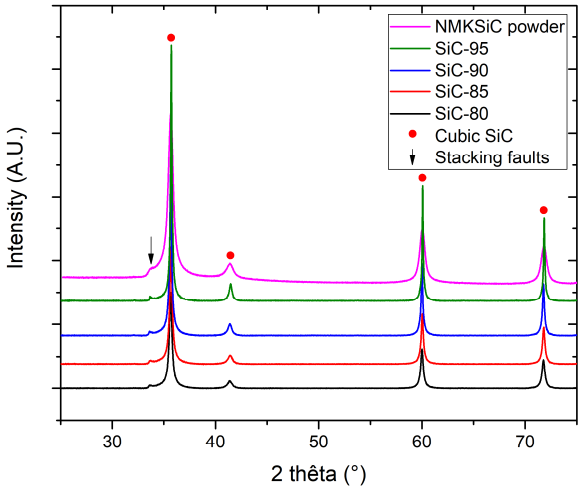

Figure 3 - Experimental XRD patterns of the pristine cubic samples denoted NMK-80, NMK-85, NMK-90 and NMK-95 compared with the one of NMKSiC powder

Hardness measurements by Knoop indentation were carried out on the four pristine cubic samples under the [25g-2000g] load range (corresponding to the [0.25-19.5N] range).

Figure 4 reports the results obtained from Knoop hardness (HK) measurements. First, it is possible to observe an important increase of hardness value when the density of the sample increases. Indeed, in the least dense samples, the presence of porosity is assimilated to defects, which could initiate brittle failure of the samples during indentation, resulting in the decrease of the hardness value. Note that the overall increase of hardness with density is observed despite an increase of grain size in the denser samples, which is generally known in the literature to decrease the hardness value of the material [10], [17]. It therefore seems that the decrease of porosity presents higher effect on the hardness value than the grain growth. However, the grain growth operating between these four samples is rather low, the densest sample presenting a grain size of about 300nm, against 150nm for the lowest dense sample. It is thus possible to suppose that the grain size difference must be much larger in order to observe a significant decrease of hardness value.

Figure 4 also highlights a gradual decrease of hardness value when the applied load increases. This decrease is then stabilized and reaches a hardness plateau. This phenomenon was already observed and described in the literature, and was reported as an Indentation Size Effect (ISE) [26]–[33]. Indeed, applying low loads only affects the local behaviour of the material (micro scale): the surface in contact with the indenter represents only few grains and very few or no defects. In this case, the response of the elastic deformation of the material is higher than the plastic one, leading to an increase of the hardness value. At the opposite,

applying high loads (as in the hardness plateau) has effects on the global behaviour of the material at the macroscopic scale: the surface in contact with the indenter involves many grains and defects and/or porosity. The plastic deformation is thus higher than the elastic response, inducing larger residual indentation print and thus lower hardness value [27].

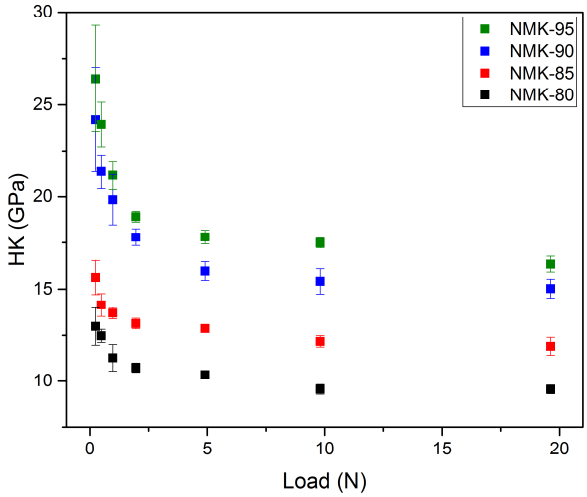

Figure 4 - Experimental hardness values of the pristine cubic samples denoted NMK-80, NMK-85, NMK-90 and NMK-95 as a function of the applied load

As the ballistic efficiency of a material relates to its global behaviour, only hardness values measured under 2000g (i.e., on the hardness plateau) will be used to determine the Young modulus and toughness in the following. This Knoop hardness will be denoted HK_2. Please note that authors in the literature do not usually determine these parameters using indentation results under 2000g. Anyway, they systematically precise the applied load during hardness tests so that comparison between various studies remains possible.

Table 2 reports the hardness values obtained from measurements on NMK-80, NMK-85, NMK-90 and NMK-95 under 2000g. They are compared to a reference SiC with a high ballistic efficiency: the Hexoloy® SA shade produced and commercialized by Saint-Gobain Company. Nevertheless, according to the technical sheets provided by the supplier, its hardness value has been determined using a 100g load, and will be denoted $HK_{0.1}$. For this reason, the comparison with the one of NMK-95 under the same load was made in this table. Please note that the Hexoloy® SA shade presents a density of about 98% (3.15 g/cm^3), according to the supplier [25].

This table testifies to the important effect of density on the hardness, with an increase of 7 GPa of the hardness value when the density increases of 15%. Nevertheless, the comparison with commercial SiC shows that, in spite of the relatively high density reached by our additive-free silicon carbide samples, they do not present a hardness as high as the Hexoloy® SA shade, which shows further higher density and a hardness value $HK_{0.1}$ of 27.5GPa larger than the 21.2GPa obtained for the sample NMK-95. It is therefore interesting to compare this reference with samples sintered from "NMKSiC powder + sintering aid" mixtures, which present densities higher than 99%. These results will be discussed in section 3.2.1.

Table 2 - Summarized table of characteristic NMKSiC samples hardness values measured under 2kg compared with that of the Hexoloy® SA SiC shade and NMKSiC-95 obtained under 0.1kg

Sample	Density	Dureté Knoop HK_2 (GPa)
NMK-80	80 ± 1%	9.6 ± 0.2
NMK-85	85 ± 1%	11.9 ± 0.5
NMK-90	90 ±1%	15.0 ± 0.5
NMK-95	95 ± 1%	16.3 ± 0.4
Hexoloy® SA	98%	27.5 ($HK_{0.1}$)
NMK-95	95 ± 1%	21.2 ± 0.8 ($HK_{0.1}$)

3.1.2 Indentation size effect

Different empirical models could be used to analyse the ISE phenomenon. The most commonly used in the literature is the Meyer's law [3]. This model is based on an exponential equation linking the load and the diagonal of the indentation:

$$P = AL^n \qquad \text{Equation 1}$$

with P the load (N), L the diagonal of the indentation (µm), A an empirical constant and n the Meyer index. Authors generally reports that the ISE phenomenon is observed when n<2 [26], [33].

It is then possible to perform a linear regression of Equation 1 by log transformation (Equation 2) and thus to fit the Meyer's law with the experimental values reported in the Figure 4.

$$\ln P = \ln A + n \times \ln L \qquad \text{Equation 2}$$

Figure 5(a) represents the linear regression performed with values obtained on the densest sample (NMK-95). This regression shows that there is a good correlation between experimental values and the Meyer's law for this sample (R^2=0.999). It is therefore possible to deduce from the straight linear regression equation the parameters A and n of the Meyer's law (respectively 76.272 and 1.805). Figure 5(b) reports all the experimental A and n parameters calculated from each characteristic sample as a function of the porosity. This Figure shows that both parameters could be interpreted by polynomial regressions respectively of 2nd and 1st degree. Starting from the hardness law (Equation 3), it is possible to obtain Equation 4 by combining it with the Meyer's law and thus deduce the A and n parameters. Replacing A and n by their polynomial expressions, one obtains the theoretical Knoop hardness (HK) value as a function of the applied load P and the porosity Φ (Equation 5).

$$HK = \frac{P}{C_p L^2} \qquad \text{Equation 3}$$

$$HK = \frac{P}{C_p \left(\frac{P}{A}\right)^{\frac{2}{n}}} \qquad \text{Equation 4}$$

$$HK = \frac{P}{C_p \left(\frac{P}{A_2\Phi^2 + A_1\Phi + A_0}\right)^{\frac{2}{n_1\Phi + n_0}}} \qquad \text{Equation 5}$$

with HK the Knoop hardness (GPa), P the load (N), C_p a constant depending on indenter geometry (C_p = 0.0703 for Knoop indenter), L the length of the great diagonal (µm), Φ the porosity, A an empirical constant et n the Meyer's index. The parameters A_0, A_1 and A_2, just as n_0 and n_1, are respectively defined as pre-factors of polynomial and linear fits of A and n parameters. They allow calculating the theoretical hardness values according to the Meyer's law as a function of the applied load for each porosity.

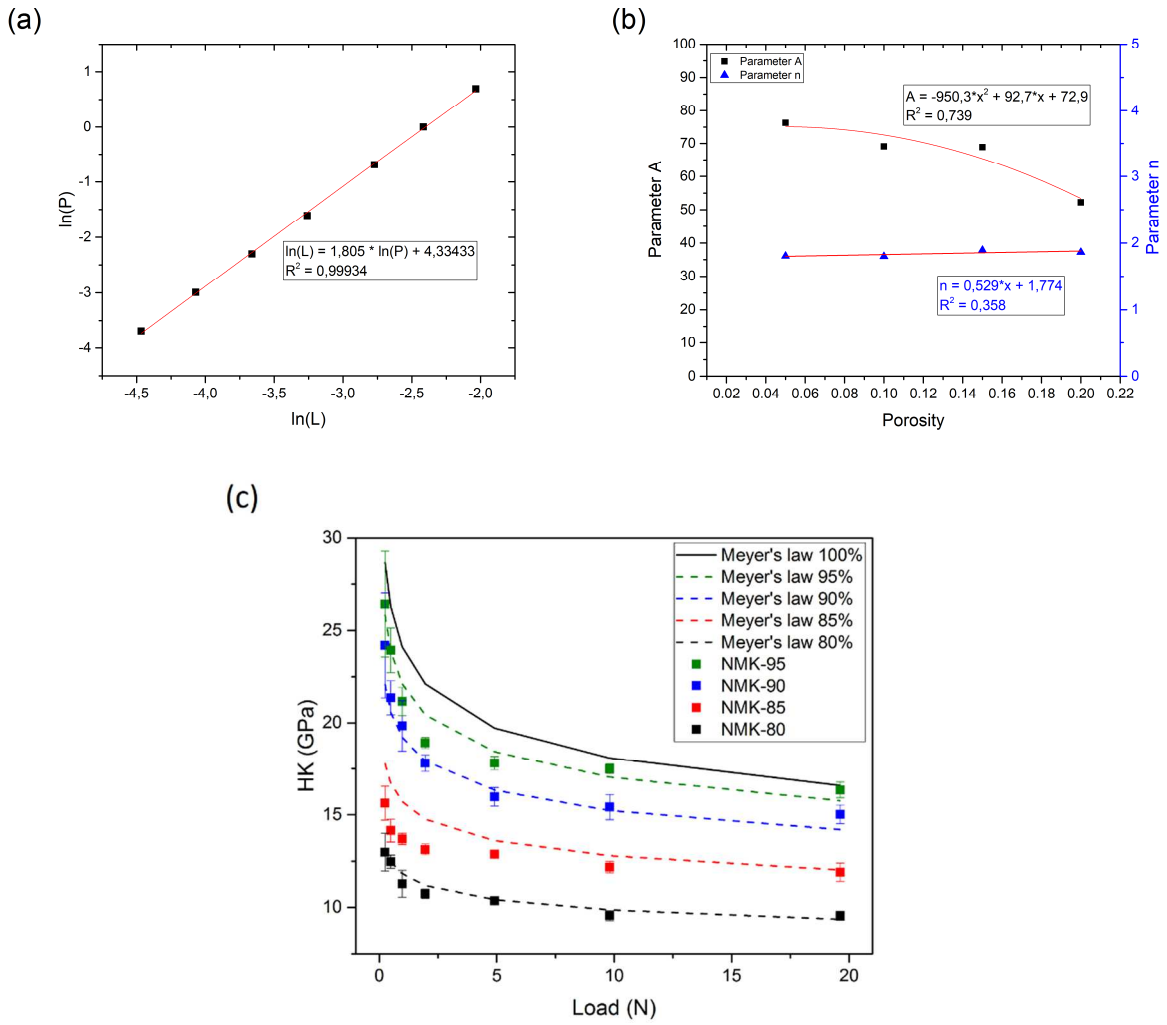

Figure 5 - Experimental results of NMKSiC samples Knoop hardness tests: (a) fitting with the Meyer's law [33], (b) A and n parameter obtained after application of the Meyer's law to the different NMKSiC samples and polynomial fits of A and n, and (c) comparison between experimental hardness values and calculated hardness values from Equation 5

The comparison between experimental hardness values and the one calculated from the two parameters of the Meyer's law is presented in Figure 5(c). It shows a good correlation between experimental values and the calculated ones for high loads (> 10N) for all the samples. It is nevertheless possible to observe a slight scattering for low loads (0-10N), particularly for samples NMK-85 and NMK-95. This lower correlation is certainly due to the low value of the coefficients of determination R^2 calculated for A and n parameters in the Figure 5(b). These results could be explained by the scattering of hardness values while applying low loads. Indeed, the relatively small indentation print could induce much large uncertainties and thus a larger scattering of measured values. Nevertheless, Young modulus and toughness being calculated with values at the hardness plateau, this scattering has no impact on their

determination. Moreover, the calculated hardness curve by the Meyer's law for a full dense sample (black curve in Figure 5(c)) is slightly higher than the one of the sample NMK-95 for all loads. This observation confirms the important effect of density on the hardness value and thus the necessity to increase the density of our sintered samples to reach the values reported in the literature.

Another empirical model could be used to establish a correlation with experimental hardness values and explain the ISE phenomenon: the Multi Fractal Scaling Law (MFSL) [29], [30], [33]. This model consists in fractal theory, explaining that different scales take part in the materials mechanics: the macro scale (global behaviour of the material), the micro scale (grains, grains boundaries and porosity) and atomic scale (dislocations). These different scales are consistent with the description by Bull et al. [27] of the evolution of hardness as a function of load and give a good explanation of the ISE phenomenon. Despite many controversies due to a lack of mechanical explanations [34], [35], this empirical theory comes from mathematical equations commonly used on many materials [29], [30], [36], [37]. This model allows to determine two parameters: HK_∞ and L*. The first one corresponds to the hardness value non-dependant of the applied load (considering a perfectly homogeneous microstructure), while the second one corresponds to a critical length of print on the material, representing the transition between the micro behaviour and the macro behaviour [29]. The MFSL thus describes the hardness of the material by the following equation:

$$HK = HK_\infty \left(1 + \frac{L^*}{L}\right)^{\frac{1}{2}} \qquad \text{Equation 6}$$

with HK the Knoop hardness (GPa), HK_∞ the hardness non-dependant of the load (GPa), L^* the transition length (µm) and L the length of the great diagonal (µm).

It is then possible to obtain the two parameters HK_∞ and L* of the MFSL for each characteristic sample from experimental hardness values by the following equation:

$$HK^2 = HK_\infty^2 + HK_\infty^2 \times L^* \times \frac{1}{L} \qquad \text{Equation 7}$$

Figure 6 reports the plotting of experimental squared hardness values as a function of 1/L in order to determine the two parameters of the MFSL. Both parameters are reported in Table 3. The latter shows HK_∞ values relatively close to the one measured under 2000g (Table 2), testifying that the hardness plateau is reached and that it represents the global behaviour of the material. It is nevertheless not possible to deduce a tendency concerning L* values as a function of porosity. Indeed, this parameter is affected by many parameters as porosity, grain

distribution but also dislocations that induce many variations and uncertainties of its value. However, the hardness tests allow measuring largest diagonals of indentation print comprised in the [11µm-17µm] range under the lowest load (25g) while this diagonal is comprised in the [130µm-170µm] range under the highest load (2kg). These results show that under low loads, the largest diagonal presents an equivalent length to the L* parameter (Table 3). This result indicates that the behaviour of the SiC material is at the border between the micro scale and the macro scale. This could also explain the wide scattering of hardness values observed under low loads. Nevertheless, these measurements confirm that the application of high loads results in L values much larger than L*, typical of a mechanical behaviour governed at the macroscopic scale. It further warrants to take the values of the hardness plateau into consideration to calculate the Young modulus and toughness properties of our samples in the following.

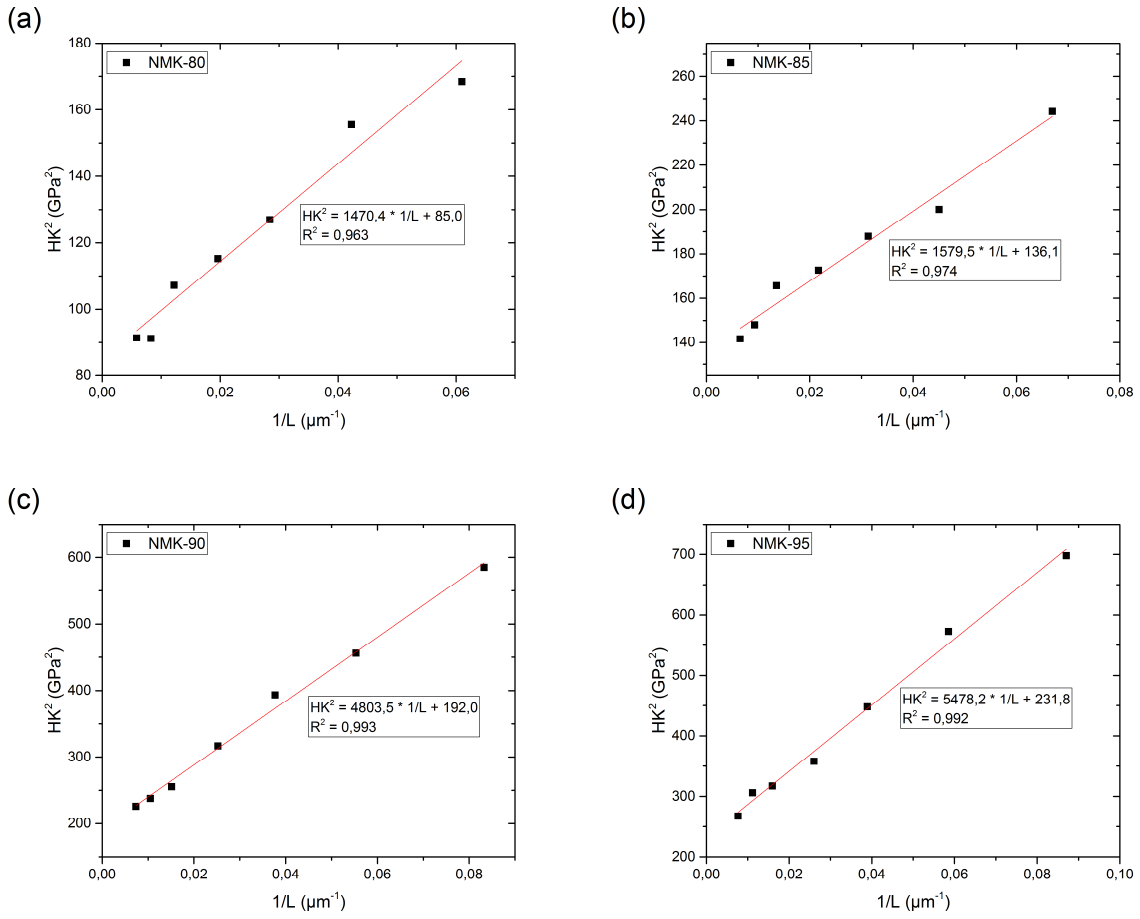

Figure 6 - Fitting of experimental Knoop hardness results of characteristic samples (a) NMK-80, (b) NMK-85, (c) NMK-90 and (d) NMK-95 with the Multi Fractal Scaling Law

Table 3 - Summarized table of HK_∞ and L^* parameters obtained from Knoop hardness measurements on the four characteristic samples NMK-80, NMK-85, NMK-90 and NMK-95

Sample	HK_∞ (GPa)	L^* (µm)
NMK-80	9.2	17.3
NMK-85	11.7	11.6
NMK-90	13.9	25.0
NMK-95	15.2	23.6

3.1.3 Young modulus

Some authors, as Krell and Strassburger, reported in the literature that Young modulus could be an interesting property during impact of a small-calibre projectile on a dual hardness armour. They explained that a material with high stiffness allows better distribution of the high-speed loading on the backing, and limits the penetration of the projectile during the first short period of the impact (< 10µs), called the dwell phase. They precise that Young modulus is only relevant during the dwell phase of the impact. Moreover, for two materials having the same hardness, the one having a higher modulus could allow expanding the dwell phase time and thus could present an improved ballistic efficiency. Nevertheless, these authors mentioned that this capacity is only valid for materials creating coarse fragments during the fragmentation phase. Then, for a material likely to form many fine fragments, as sapphire, the increase of Young modulus for a given hardness does not lead to a significant improvement of ballistic efficiency [38], [39].

The Young modulus calculation could be performed from HK measurements. Indeed, several studies in the literature, as the one of Marshall, showed that there is a relation linking the Young modulus E and the small/great print diagonal ratio [18]:

$$E = \frac{\alpha'' \times HK}{\frac{b}{x} - \frac{b'}{x'}} \qquad \text{Equation 8}$$

with b' and x' respectively the lengths of the shortest and largest diagonal measured on the residual Knoop print, $\frac{b}{x}$ close to $\frac{1}{7}$ for a Knoop indenter, α'' a constant with the value of 0.45 and HK the Knoop hardness (GPa). The b and x values correspond to the Knoop print sizes during load application, and the $\frac{b}{x}$ ratio is accordingly defined thanks to the indenter geometry.

The Young modulus values of the different SiC samples were determined from the latter equation. The results are reported in Figure 7(a) as a function of residual porosity. They show

an increase of the Young modulus according to the decrease of porosity, which is consistent with the Spriggs' Law (Equation 9), featuring an exponential evolution of the Young modulus as a function of porosity [40].

The Sprigg's law writes

$$E = E_0 e^{-b\Phi} \qquad \text{Equation 9}$$

with E_0 the theoretical value of SiC Young modulus (without porosity), b an empirical parameter and Φ the porosity.

Nevertheless, the exponential regression performed on experimental values allows determining a Young modulus value of SiC without porosity of about 280GPa, which is significantly lower than the one generally reported in the literature (460GPa for the theoretical value) [39]. This difference certainly comes from the measurement method, which could induce many uncertainties (inaccurate assessment of the shortest diagonal length) and underestimate Young modulus values of samples sintered in this work. It is therefore necessary to follow another approach to get more relevant Young modulus measurements.

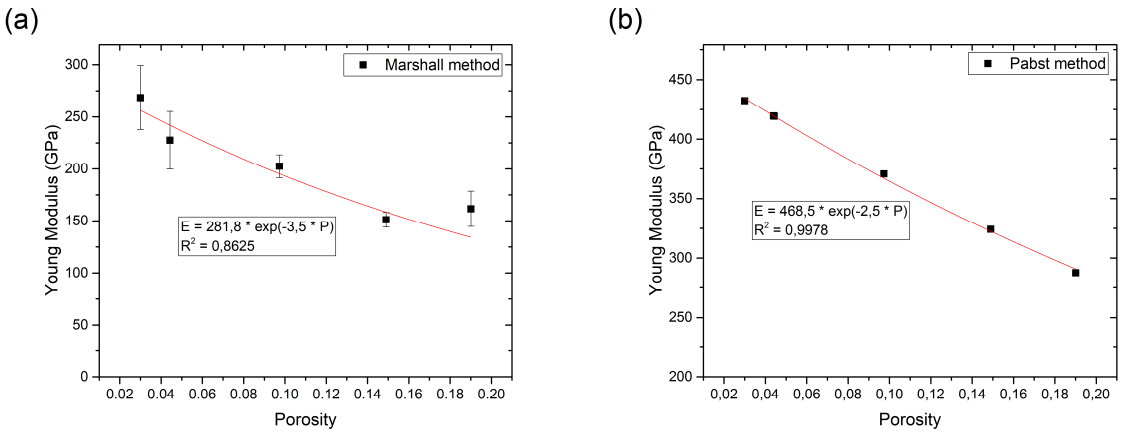

Figure 7 - Evolution of Young Modulus values of SiC samples as a function of density calculated from (a) Marshall's method [18] and (b) Pabst's method [19]. The plain curves correspond to fittings with the Sprigg's law.

Other studies showed that the factor having the most important impact on the Young modulus is the porosity of the material. It is then possible to determine this property from the Pabst's relation, as described by Equation 10 [19].

$$E = E_0 e^{\frac{-2\Phi}{1-\Phi}}$$ Equation 10

with E_0 the theoretical value of SiC Young modulus (without porosity, generally 460GPa), b an empirical parameter and Φ the porosity. Young modulus values calculated from this equation are presented in Figure 7(b) as a function of porosity.

As already observed, the Young modulus of SiC describes a growing evolution when the porosity decreases. Nevertheless, the values calculated with the Pabst's equation are significantly higher than the ones obtained with the Marshall' law (Equation 8 [30]). Fitting the observed exponential regression with the Sprigg's law logically results in a Young modulus of dense SiC of about 468.5GPa, i.e. close to the theoretical value (460GPa) [39], with a coefficient of determination R^2 of 0.998. Following this approach, the elastic modulus of our densest SiC sample (NMK-95) reaches 419GPa. This is encouraging compared to results reported in the literature for Spark Plasma Sintered SiC. Indeed, authors generally report Young modulus values from 410GPa (Hexoloy® SA shade) to 442GPa for highly dense SiC (99%) sintered by SPS in solid state [24].

These results indicate that the Pabst's relation could allow obtaining a more reliable value of the Young modulus than the Marshall's equation, which probably depends on too many physical factors not taken into account in the equation (porosity, dislocation …). The Young modulus calculation will be performed using Equation 10 in the following.

3.1.4 Toughness

The toughness K_{IC} of a material represents its capacity to block cracks spreading in mode I (tensile strain perpendicular to cracks plan), and corresponds to the quantity of energy that the material can absorb before breaking. This property is therefore extremely important during the fragmentation phase of the projectile impact.

Toughness values of spark plasma sintered SiC samples were calculated from Vickers hardness tests, after measurement of print diagonals and cracks that appear all around it [20]–[22]. Niihara et al. demonstrated that there were several models to determine toughness according to the kind of cracks: "median" or "Palmqvist" cracks [20], [23]. These authors reported the possibility to determine the kind of cracks thanks to the $\frac{c'}{a}$ or $\frac{l'}{a}$ ratio (with c' and l' the mean value of respectively median cracks and Palmqvist cracks, and a the mean length of diagonals). Indeed, if this ratio is higher than 2.5, cracks are median cracks, while if the ratio is lower than 2.5, they are Palmqvist cracks.

Table 4 reports Vickers hardness measurements performed on samples NMK-80, NMK-85, NMK-90 and NMK-95, compared with the values reported in the literature for the Hexoloy® SA shade [24], [25] and for another SiC pellet sintered by SPS in solid state (called SPS-S) [24]. Toughness calculations were thus carried out by Equation 11.

$$K_{IC} = 0.067 \times \left(\frac{E}{HV}\right)^{0.4} \times HV \times a^{\frac{1}{2}} \times \left(\frac{c\prime}{a}\right)^{-\frac{3}{2}} \qquad \text{Equation 11}$$

with E the Young modulus derived from equation 10, HV the Vickers hardness, a the mean length of diagonals and c' the mean value of cracks. Please note that these measurements allowed highlighting median cracks.

Table 4 – Experimental Vickers hardness values obtained under 1 kg (HV_1) and 2kg (HV_2) and calculated toughness values of the four characteristic pristine cubic samples from Vickers assays under 2 kg, compared with the ones of Hexoloy® SA SiC shade and SPS-S under 1kg

Sample	Density	HV_1 (GPa)	HV_2 (GPa)	Kind of cracks	Toughness ($MPa.m^{-1/2}$)
NMK-80	80 ± 1%	12.2 ± 0.4	11.4 ± 0.3	Median	4.0 ± 0.2
NMK-85	85 ± 1%	14.6 ± 0.5	13.4 ± 0.4	Median	4.5 ± 0.3
NMK-90	90 ± 1%	22.1 ± 0.9	19.7 ± 1.3	Median	3.9 ± 0.2
NMK-95	95 ± 1%	23.7 ± 1.1	23.2 ± 0.7	Median	4.4 ± 0.5
Hexoloy® SA	96.6%	24.3	-	-	4.6
SPS-S	99%	27	-	-	2.5

This table shows, as for Knoop experimentations, a growing evolution of Vickers hardness values according to the density. Please note that the evolution of these values also presents an ISE phenomenon for all samples (decrease of hardness according to an increase of load). The Vickers measurements presented here (HV_1 and HV_2) are thus located in the hardness plateau. However, these results show hardness values lower than the one reported in the literature for a SiC sample sintered by SPS (23.7GPa against 27GPa [24]). This difference of hardness could certainly come from the difference of density between these two samples. It is nevertheless possible to notice that our densest sample (NMK-95) shows a hardness close to the one of the Hexoloy® SA shade. Despite lower Vickers hardness values, all the samples sintered in this study show a toughness similar to the one of Hexoloy® SA shade, and higher than the one of another sample reported in the literature (SPS-S). This high toughness let us anticipate a good fragmentation behaviour of our sample NMK-95.

Figure 8 shows the evolution of toughness of samples sintered in this work as a function of porosity. Whereas some studies reported an impact of porosity on the toughness value [41], these results seem to indicate a relatively constant toughness, regardless of the porosity. It is also shown that a slight change of grain size (from 150nm to 320nm) seems to have no influence on toughness, contrarily to what was reported by several authors in the literature who demonstrated a slight decrease of fracture toughness while grain size increases from 150nm up to 17µm [42], [43].

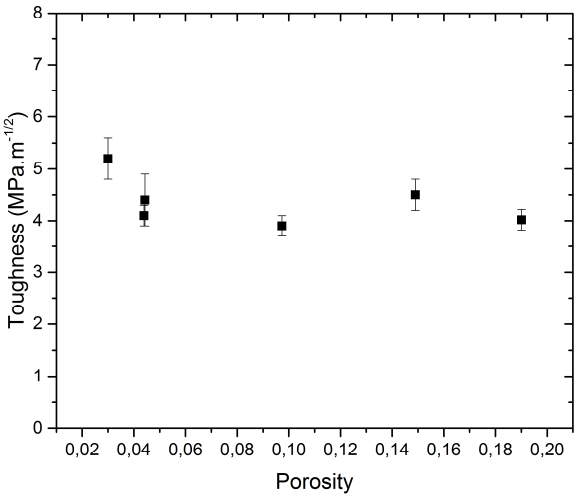

Figure 8 - Evolution of toughness values of SiC samples as a function of porosity

The different hardness characterizations on the NMK-80, NMK-85, NMK-90 and NMK-95 samples highlighted lower Knoop and Vickers hardness values than the ones reported in the literature. It has however been demonstrated that these values can be explained by the higher densities of referenced samples in the literature. Moreover, it was possible to reach toughness and Young modulus values equivalent to the ones reported in the literature and even higher in the case of sample NMK-95. These results show that our SPS SiC materials present high stiffness and toughness, suggesting a good capacity to fragmentation and thus an interesting ballistic efficiency.

3.2 Sintered samples with sintering aids

In parallel, SiC pellets were sintered with the addition of low content (0.5wt %) of sintering aids in order to increase their density while limiting the presence of secondary phases. Three compounds were used to prepare the different “NMKSiC powder + sintering aids” mixtures:

Al_2O_3, Al_2O_3/Y_2O_3 (respectively mixed with 0.63 and 0.37 content) and Al_2O_3/AlN (respectively mixed with 0.50 and 0.50 content). The Table 5 reports the different characteristics of the studied doped samples.

Table 5 - Summarized table of the different tested doped SiC samples

Sample	Sintered aid	Sintering pressure (MPa)	Density (%)	Grain size (µm)
NMK17-NA50	Al_2O_3/AlN	17	99 ± 1%	n.a.
NMK80-NA50	Al_2O_3/AlN	80	98 ± 1%	290
NMK127-NA50	Al_2O_3/AlN	127	99 ± 1%	500
NMK80-A50	Al_2O_3	80	99 ± 1%	610
NMK80-AY50	Al_2O_3/Y_2O_3	80	98 ± 1%	320

3.2.1 Hardness measurements

Knoop hardness measurements were carried out on the different samples sintered from "NMKSiC powder + sintering aids" mixtures. As we demonstrated in the latter section on the influence of porosity on hardness values, it was decided to characterize here only the densest cubic samples in order to compare with the dense samples reported in the literature. In addition, one of the objectives of this work being the development of cubic samples without secondary phases, only sintered samples with very low sintering aids contents of 0.5wt% will be considered in the following.

The addition of the NA (Al_2O_3-AlN mixture) component enabled to obtain equivalent densities (98-99%) regardless of the sintering pressure for an amount of 0.5wt% of sintering aid. Knoop hardness measurements were carried out on the three samples NMK-NA50, NMK80-NA50 and NMK127-NA50 in order to firstly evaluate the impact of the sintering pressure (respectively 17, 80 and 127MPa) and also the microstructure (grain size and porosity) on the hardness of the material doped with the same component. Figure 9 shows the experimental results obtained as a function of the applied load.

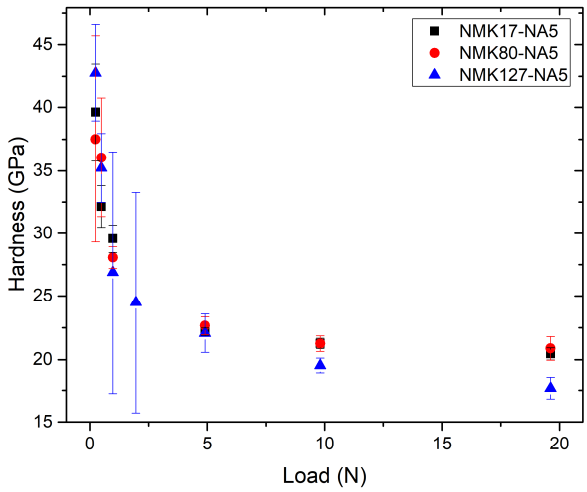

Figure 9 - Experimental Knoop hardness values of NMK17-NA50, NMK80-NA50 and NMK127-NA50 samples

This figure shows a decrease of the hardness values with the increase of the load for each sample, confirming the ISE phenomenon. The three samples exhibit equivalent results for low loads (micro scale) up to 5N with, nonetheless, a wider scattering of the measurements for the sample sintered at 127MPa. However, the latter sample presents hardness values lower than those measured for the samples NMK17-NA50 and NMK80-NA50 under high load (9.8N and 19.6N). These results appear for the macro scale behaviour and could be explained by the global microstructure of the material. Indeed, Figure 10 (a) and (b) show that the sample sintered under 80MPa has a very fine and well-distributed porosity, whereas the sample NMK127-NA50 has a coarser porosity randomly distributed. This porosity could be related to a significant size of defect which appears to be critical for hardness properties [17]. Moreover, the increase of the sintering pressure induced a grain growth (500nm versus 290nm), thus explaining the decrease of the hardness (17.7GPa versus 20.9GPa for NMK80-NA50). Indeed, certain authors have demonstrated higher hardness values associated with a finer microstructure [10].

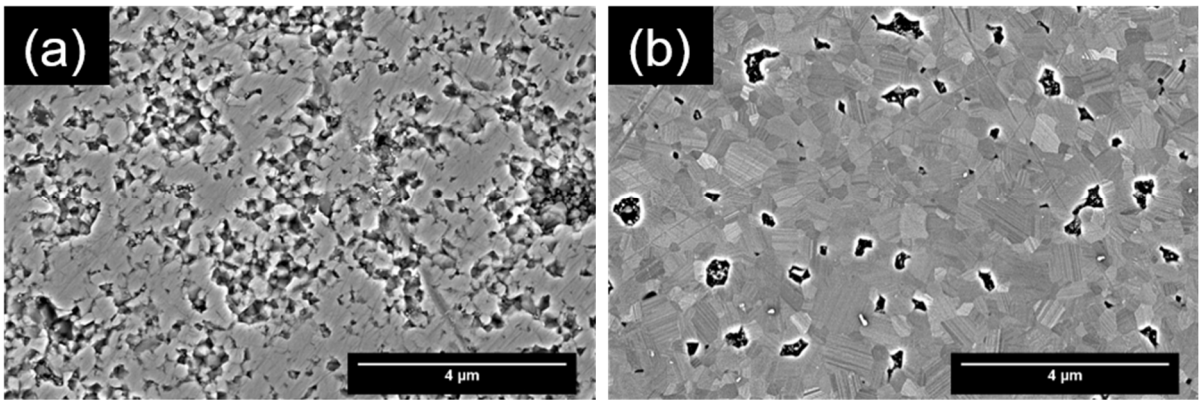

Figure 10 - SEM micrographs of the samples (a) NMK80-NA50 and (b) NMK127-NA50

Figure 9 also shows that the hardness values of the samples NMK17-NA50 and NMK80-NA50 respectively reach 20.5GPa and 20.9GPa under 2kg. The addition of 0.5wt% of NA mixture therefore allows a 4% increase of the density in regards to the sample NMK-95, improving the hardness value by 5GPa to reach more than 20GPa. These results also reveal higher hardness values compared to the ones reported in the literature, particularly the Hexoloy® SA shade, which presents a hardness of 27.5GPa under 0.1kg against 28-29GPa for our samples. These observations suggest encouraging ballistic efficiency values.

Other hardness experiments were performed on samples sintered from mixtures with sintering aids in order to observe the influence of the nature of additive on hardness. Figure 11 reports experimental results obtained from measurements on samples NMK80-A50, NMK80-AY50 and NMK80-NA50. This figure shows that these three samples present an ISE phenomenon. It is possible to note hardness values of respectively 20.9GPa, 20.5GPa and 17.2GPa for samples doped with the NA50, A50 and AY50 mixtures. These results also reveal lower values of hardness for the sample sintered from AY50 mixture for all applied loads. This observation indicates that the addition of this additive is likely to weaken the SiC material despite of a relatively fine microstructure.

Hardness values of samples doped with A50 and NA50 mixtures seem to be equivalent, taking into account measurements errors. These results demonstrate that samples sintered in this work with only low content of sintering aids present higher density than the Hexoloy® SA shade (99% against 96.6% for the commercial SiC), and therefore better aptitude for ballistic applications.

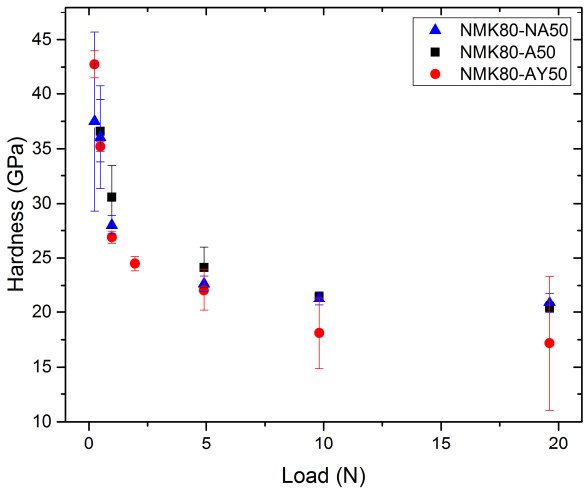

Figure 11 - Experimental Knoop hardness values of NMK80-A50, NMK80-AY50 and NMK80-NA50 samples

3.2.2 Young modulus

As described in section 3.1.3, Young modulus calculation of samples sintered from sintering aids mixtures is based on the Pabst relation (Equation 10) [19]. Table 6 reports calculated modulus values for samples presenting the highest hardnesses. These results are compared with two SiC samples referenced in the literature as presenting high ballistic performances: the Hexoloy® SA shade of Saint-Gobain and a sample sintered by SPS in liquid-state and called SPS-L [44]. The comparison with the latter sample (preferred to the SPS-S sample mentioned above) was done in order to be relevant with the results of our samples, which have been sintered in liquid-state thanks to the addition of sintering aids.

Table 6 - Young Modulus values of sintered samples from "SiC powder + sintering aids" mixtures compared with that of Hexoloy® SA SiC shade and SPS-L

Sample	Density	Young modulus (GPa)
NMK80-A50	99 ± 1%	450.8
NMK17-NA50	99 ± 1%	450.8
NMK80-NA50	99 ± 1%	441.6
NMK80-NA25	99 ± 1%	450.8
Hexoloy® SA	96.6 ± 1%	410
SPS-L	99%	410

This table reveals equivalent, and even higher, values of Young modulus for the SPS ceramics of the study compared to the SiC referenced in the literature. These properties could lead to longer dwell phase during the impact and thus let suppose an improved efficiency of the ceramic.

3.2.3 Toughness

As for samples sintered without any sintering aids, Vickers hardness measurements were performed on doped samples in order to evaluate their toughness. These measurements were carried out on the most promising samples regarding mechanical properties, namely NMK80-A50, NMK17-NA50, NMK80-NA50 and NMK80-NA25, and are summarized in Table 7.

Vickers hardness measurements revealing median cracks for each sample, toughness values were calculated from Equation 11 and were introduced in Table 7 along with the ones from the two references, i.e. the Hexoloy® SA shade of Saint-Gobain and the SPS-L sample.

Table 7 - Experimental HV_2 and calculated toughness values of doped samples compared with the HV_1 and toughness of Hexoloy® SA SiC shade and SPS-L.

Sample	Density	HV_1 (GPa)	HV_2 (GPa)	Kind of cracks	Toughness ($MPa.m^{-1/2}$)
NMK80-A50	99 ± 1%	-	29.7 ± 2.2	Median	5.3 ± 2
NMK17-NA50	99 ± 1%	-	30.9 ± 1.7	Median	5.1 ± 1.8
NMK80-NA50	99 ± 1%	-	30.1 ± 2.2	Median	5.6 ± 2.3
NMK80-NA25	99 ± 1%	-	30.5 ± 2.3	median	5.1 ± 1.7
Hexoloy® SA	96.6 ± 1%	24.3	-	-	4.6
SPS-L	99%	23.9	-	-	3.8

This table reports Vickers hardness and toughness values relatively similar, respectively of about 30GPa and 5MPa.$m^{1/2}$ for all the doped samples of this study. The scattering of hardnesses and toughness values could certainly come from the presence of secondary phases due to the sintering additive. Indeed, the added components present lower hardness than that of pure SiC. The addition of these aids could improve hardness of sintered samples thanks to the increase of density. Nevertheless, their low content, and thus their presence in the sample, could induce a dispersion of the measurement results according to their presence/absence at the indentation print.

These results also show that the samples sintered in this work present a Vickers hardness 6GPa higher than the one of SiC referenced in the literature, despite a higher applied load. Although errors bars are rather large, the toughness of our samples appears equivalent, and even higher (about 1-2 MPa.$m^{1/2}$), than that of the Hexoloy® SA shade and of the SPS-L pellet.

The hardness results obtained for samples sintered with the undoped NMKSiC powder and the SiC mixed with sintering aids A and NA ((Al_2O_3 and Al_2O_3-AlN) reveal encouraging properties for ballistic application. Indeed, in spite of slightly lower hardness values, samples sintered from undoped powders show Young modulus and toughness higher than the SiC references for ballistic protection quoted in the literature. Moreover, the addition of very low contents of sintering aids allows improving greatly these properties, rendering cubic SiC further more promising for ballistic applications.

4 Conclusion

The Knoop and Vickers hardness as well as physical properties (Young modulus and toughness) of cubic SiC samples sintered by SPS were studied.

These measurements allowed us to demonstrate the strong influence of the porosity on the hardness value. We have highlighted that the increase of the load during the indentation measurements resulted in the appearance of an indentation size effect that was described and commented. The impact of porosity on the Young modulus calculation was also shown in this paper. Two models were considered in order to derive the Young modulus from indentation assays, namely the Marshall's and the Pabst's model, and we showed that only the second one was able to give more reliable results.

The results obtained on the densest of our pure SiC samples were found to be very encouraging, particularly concerning Young modulus and toughness, in order to develop tiles with high ballistic efficiency. Moreover, the characterization of samples sintered with very low content of additive revealed widely improves mechanical properties. Indeed, thanks to densities higher than 99%, these samples presented Knoop hardness reaching almost 30GPa under 0.1kg, a toughness of about 5MPa.$m^{1/2}$ and even an elastic modulus close to the theoretical value (450GPa). For some materials, these results showed higher mechanical properties than the ones reported in the literature by various authors concerning SiC developed for ballistic protection. Upon scaling up our set-up for the production of larger pellets, our SPS SiC samples could have inedited performance in ballistic protection applications.

Acknowledgements

F. Delobel is now working as researcher in the Belgian Ceramic Research Centre (Mons).

The authors thank the ISL (French-German Research Institute of Saint-Louis) for funding on silicon carbide ceramics development, F. Moitrier for X-ray diffraction analyses, J. Sampaio for hardness measurements and Dr. R. D'Elia for scientific discussions. Bundesamt für Ausrüstung, Informationstechnik und Nutzung der Bundeswehr (BAAINBw) and Wehrwissenschaftliches Institut für Werk- und Betriebsstoffe (WIWeB) are thanked for their support.

References

[1] R. Riedel, Ed., *Handbook of Ceramic Hard Materials*. Weinheim, Germany: Wiley-VCH Verlag GmbH, 2000.

[2] Ceramic Armor Materials by Design Symposium, J. W. McCauley, and Pac Rim IV International Conference on Advanced Ceramics and Glass, *Ceramic armor materials by design: proceedings of the Ceramic Armor Materials by Design Symposium held at the Pac Rim IV International Conference on Advanced Ceramics and Glass, November 4-8, 2001 in Wailea, Maui, Hawaii*. Westerville, Ohio: American Ceramic Society, 2002.

[3] M. Chen, 'Shock-Induced Localized Amorphization in Boron Carbide', *Science*, vol. 299, no. 5612, pp. 1563–1566, Mar. 2003, doi: 10.1126/science.1080819.

[4] *Silicon Carbide–1968*. Elsevier, 1969.

[5] V. V. Pujar, R. P. Jensen, and N. P. Padture, 'Densification of liquid-phase-sintered silicon carbide', *Journal of Materials Science Letters*, vol. 19, no. 11, pp. 1011–1014, 2000, doi: 10.1023/A:1006753213286.

[6] Y.-W. Kim, M. Mitomo, and G.-D. Zhan, 'Mechanism of grain growth in liquid-phase-sintered β–SiC', *Journal of Materials Research*, vol. 14, no. 11, pp. 4291–4293, Nov. 1999, doi: 10.1557/JMR.1999.0581.

[7] A. Kaiser, R. Vassen, D. Stöver, and H. P. Buchkremer, 'Heat treatment of ultrafine SiC powders to reduce oxidation sensitivity and grain growth', *Nanostructured Materials*, vol. 4, no. 7, pp. 795–802, Jan. 1994, doi: 10.1016/0965-9773(94)90085-X.

[8] B. Lanfant *et al.*, 'Effects of carbon and oxygen on the spark plasma sintering additive-free densification and on the mechanical properties of nanostructured SiC ceramics', *Journal of the European Ceramic Society*, vol. 35, no. 13, pp. 3369–3379, Nov. 2015, doi: 10.1016/j.jeurceramsoc.2015.05.014.

[9] C. Lorrette, A. Réau, and L. Briottet, 'Mechanical properties of nanostructured silicon carbide consolidated by spark plasma sintering', *Journal of the European Ceramic Society*, vol. 33, no. 1, pp. 147–156, Jan. 2013, doi: 10.1016/j.jeurceramsoc.2012.07.030.

[10] R. Vassen, A. Kaiser, J. Förster, H. P. Buchkremer, and D. Stöver, 'Densification of ultrafine SiC powders', *Journal of Materials Science*, vol. 31, no. 14, pp. 3623–3637, 1996, doi: 10.1007/BF00352770.

[11] R. Vassen and D. Stöver, 'Processing and Properties of Nanograin Silicon Carbide', *Journal of the American Ceramic Society*, vol. 82, no. 10, pp. 2585–2593, Dec. 2004, doi: 10.1111/j.1151-2916.1999.tb02127.x.

[12] H. N. Baumann, 'The Relationship of Alpha and Beta Silicon Carbide', *Journal of The Electrochemical Society*, vol. 99, no. 3, p. 109, 1952, doi: 10.1149/1.2779671.

[13] N. W. Jepps and T. F. Page, 'Polytypic transformations in silicon carbide', *Progress in Crystal Growth and Characterization*, vol. 7, no. 1–4, pp. 259–307, Jan. 1983, doi: 10.1016/0146-3535(83)90034-5.

[14] V. K. Kabra, D. Pandey, and S. Lele, 'A diffraction approach for the study of the mechanism of 3C to 6H transformation in SiC', *Journal of Materials Science*, vol. 21, no. 5, pp. 1654–1666, May 1986, doi: 10.1007/BF01114722.

[15] S. Sugiyama and M. Togaya, 'Phase Relationship between 3C- and 6H-Silicon Carbide at High Pressure and High Temperature', *Journal of the American Ceramic Society*, vol. 84, no. 12, pp. 3013–3016, Dec. 2001, doi: 10.1111/j.1151-2916.2001.tb01129.x.

[16] F. Delobel, S. Lemonnier, É. Barraud, and J. Cambedouzou, 'Influence of sintering temperature and pressure on the 3C-6H transition of silicon carbide', *Journal of the European Ceramic Society*, vol. 39, no. 2–3, pp. 150–156, Feb. 2019, doi: 10.1016/j.jeurceramsoc.2018.09.010.

[17] N. Petch, 'The cleavage strength of polycrystals', *Journal of the Iron and Steel Institute*, vol. 174, pp. 25–28, 1953.

[18] D. B. Marshall, T. Noma, and A. G. Evans, 'A Simple Method for Determining Elastic-Modulus–to-Hardness Ratios using Knoop Indentation Measurements', *Journal of the*

American Ceramic Society, vol. 65, no. 10, pp. c175–c176, 1982, doi: 10.1111/j.1151-2916.1982.tb10357.x.

[19] W. Pabst, E. Gregorová, and G. Tichá, 'Elasticity of porous ceramics—A critical study of modulus–porosity relations', *Journal of the European Ceramic Society*, vol. 26, no. 7, pp. 1085–1097, Jan. 2006, doi: 10.1016/j.jeurceramsoc.2005.01.041.

[20] K. Niihara, R. Morena, and D. P. H. Hasselman, 'Evaluation ofK Ic of brittle solids by the indentation method with low crack-to-indent ratios', *Journal of Materials Science Letters*, vol. 1, no. 1, pp. 13–16, Jan. 1982, doi: 10.1007/BF00724706.

[21] G. R. Anstis, P. Chantikul, B. R. Lawn, and D. B. Marshall, 'A Critical Evaluation of Indentation Techniques for Measuring Fracture Toughness: I, Direct Crack Measurements', *Journal of the American Ceramic Society*, vol. 64, no. 9, pp. 533–538, Sep. 1981, doi: 10.1111/j.1151-2916.1981.tb10320.x.

[22] A. G. Evans and E. A. Charles, 'Fracture Toughness Determinations by Indentation', *Journal of the American Ceramic Society*, vol. 59, no. 7–8, pp. 371–372, Jul. 1976, doi: 10.1111/j.1151-2916.1976.tb10991.x.

[23] K. Niihara, 'A fracture mechanics analysis of indentation-induced Palmqvist crack in ceramics', *Journal of Materials Science Letters*, vol. 2, no. 5, pp. 221–223, May 1983, doi: 10.1007/BF00725625.

[24] J.-L. Zinszner, B. Erzar, and P. Forquin, 'Shockless Characterization of Ceramics Using High-Pulsed Power Technologies', in *Dynamic Damage and Fragmentation*, John Wiley & Sons, Ltd, 2019, pp. 365–385.

[25] 'Hexoloy SA | Alpha Silicon Carbide | Manufacturer'. [Online]. Available: https://www.ceramicsrefractories.saint-gobain.com/hexoloy/sa-grade. [Accessed: 22-Jan-2019].

[26] E. Meyer, 'Untersuchen uber Harteprufung und Harte', *Zeitschrift des Vereins Deutschen Ingenieure*, vol. 52, p. 645, 1908.

[27] S. J. Bull, T. F. Page, and E. H. Yoffe, 'An explanation of the indentation size effect in ceramics', *Philosophical Magazine Letters*, vol. 59, no. 6, pp. 281–288, Jun. 1989, doi: 10.1080/09500839908206356.

[28] J. Gong, J. Wu, and Z. Guan, 'Examination of the indentation size effect in low-load vickers hardness testing of ceramics', *Journal of the European Ceramic Society*, vol. 19, no. 15, pp. 2625–2631, Nov. 1999, doi: 10.1016/S0955-2219(99)00043-6.

[29] A. Carpinteri and S. Puzzi, 'A fractal approach to indentation size effect', *Engineering Fracture Mechanics*, vol. 73, no. 15, pp. 2110–2122, Oct. 2006, doi: 10.1016/j.engfracmech.2006.04.020.

[30] A. Carpinteri and S. Puzzi, 'The fractal-statistical approach to the size-scale effects on material strength and toughness', *Probabilistic Engineering Mechanics*, vol. 24, no. 1, pp. 75–83, Jan. 2009, doi: 10.1016/j.probengmech.2008.01.003.

[31] J. J. Swab *et al.*, 'Knoop Hardness–Apparent Yield Stress Relationship in Ceramics', *International Journal of Applied Ceramic Technology*, vol. 9, no. 3, pp. 650–655, 2012, doi: 10.1111/j.1744-7402.2011.02686.x.

[32] C. D. Hilton, J. W. McCauley, J. J. Swab, E. R. Shanholtz, and M. W. Chen, 'Using Hardness Tests to Quantify Bulk Plasticity and Predict Transition Velocities in SiC Materials', *International Journal of Applied Ceramic Technology*, vol. 10, no. 1, pp. 114–122, Jan. 2013, doi: 10.1111/j.1744-7402.2012.02817.x.

[33] E. R. Shanholtz and J. C. LaSalvia, 'Investigation of the Indentation-Size Effect (ISE) in a Commercial SiAlON: Multifractal Scaling Analysis and Underlying Mechanisms', *Journal of the American Ceramic Society*, vol. 96, no. 8, pp. 2607–2614, Aug. 2013, doi: 10.1111/jace.12450.

[34] Z. P. BAŽANT, 'Scaling of quasibrittle fracture: asymptotic analysis', *International Journal of Fracture*, vol. 83, no. 1, p. 19, Jan. 1997, doi: 10.1023/A:1007387823522.

[35] Z. P. BaŽant, 'Scaling of quasibrittle fracture: hypotheses of invasive and lacunar fractality, their critique and Weibull connection', *International Journal of Fracture*, vol. 83, no. 1, p. 41, Jan. 1997, doi: 10.1023/A:1007335506684.

[36] B. B. Mandelbrot, ‘The fractal geometry of nature/Revised and enlarged edition’, *New York, WH Freeman and Co., 1983, 495 p.*, 1983.
[37] A. Carpinteri and N. Pugno, ‘Are scaling laws on strength of solids related to mechanics or to geometry?’, *Nature Materials*, vol. 4, pp. 421–423, Jun. 2005, doi: 10.1038/nmat1408.
[38] A. Krell and E. Strassburger, ‘Order of influences on the ballistic resistance of armor ceramics and single crystals’, *Materials Science and Engineering: A*, vol. 597, pp. 422–430, Mar. 2014, doi: 10.1016/j.msea.2013.12.101.
[39] L. L. Snead, T. Nozawa, Y. Katoh, T.-S. Byun, S. Kondo, and D. A. Petti, ‘Handbook of SiC properties for fuel performance modeling’, *Journal of Nuclear Materials*, vol. 371, no. 1–3, pp. 329–377, Sep. 2007, doi: 10.1016/j.jnucmat.2007.05.016.
[40] R. M. Spriggs, ‘Expression for Effect of Porosity on Elastic Modulus of Polycrystalline Refractory Materials, Particularly Aluminum Oxide’, *Journal of the American Ceramic Society*, vol. 44, no. 12, pp. 628–629, Dec. 1961, doi: 10.1111/j.1151-2916.1961.tb11671.x.
[41] A. Atkinson, P. Bastid, and Q. Liu, ‘Mechanical Properties of Magnesia?Spinel Composites’, *Journal of the American Ceramic Society*, vol. 90, no. 8, pp. 2489–2496, Aug. 2007, doi: 10.1111/j.1551-2916.2007.01733.x.
[42] T. A. Yamamoto, T. Kondou, Y. Kodera, T. Ishii, M. Ohyanagi, and Z. A. Munir, ‘Mechanical Properties of β-SiC Fabricated by Spark Plasma Sintering’, *Journal of Materials Engineering and Performance*, vol. 14, no. 4, pp. 460–466, Aug. 2005, doi: 10.1361/105994905X56250.
[43] B. M. Moshtaghioun, D. Gomez-Garcia, A. Dominguez-Rodriguez, and Richard. I. Todd, ‘Grain size dependence of hardness and fracture toughness in pure near fully-dense boron carbide ceramics’, *Journal of the European Ceramic Society*, vol. 36, no. 7, pp. 1829–1834, Jun. 2016, doi: 10.1016/j.jeurceramsoc.2016.01.017.
[44] G. Rossiquet, ‘Carbure de silicium pour application blindage: élaboration et étude du comportement à l’impact’, PhD Thesis, Dijon, 2012.